Expert Systems With Applications 291 (2025) 128536

Contents lists available at ScienceDirect

Expert Systems With Applications

journal homepage: www.elsevier.com/locate/eswa

Cardiac index adaptive physiological control system for continuous-flow left ventricular assist device

Hongtao Liu [a,1,*], Aili Guan [b,1], Fayu Xing [c,1], Yunpeng Zhang [d], Wencheng Wang [a], Guoxu Liu [e]

[a] School of Machinery and Automation, Weifang University, Weifang, 261061, China
[b] Department of Cardiology, Heart Center, Qingdao Municipal Hospital, University of Health and Rehabilitation Sciences, Qingdao, 261061, China
[c] Goertek College of Science and Technology Industry, Weifang University, Weifang, 261061, China
[d] School of Electrical Engineering, Shandong University, Jinan, 250061, China
[e] School of Computer Engineering, Weifang University, Weifang, 261061, China

ARTICLE INFO

Keywords:
Cardiac index
Physiological control
Regulator
Adaptive controller
Personalized therapy

ABSTRACT

A personalized continuous-flow left ventricular assist device (CFLVAD) therapy is designed to provide a precise treatment strategy based on the specific circumstances and needs of the individual patient. The aim is to improve treatment outcomes and the patient's quality of life. Given this background, this study proposes a cardiac index adaptive physiological control (CIAPC) strategy to personalize the CFLVAD therapy. The CFLVAD physiological control system was constructed based on the cardiovascular coupling system model. A cardiac index regulator was designed by deriving a functional relationship between cardiac index and heart rate, height, and weight. The cardiac index adaptive controller consisted of the cardiac index regulator combined with a fuzzy controller and a ventricular suction prevention controller. The rotary pump flow and left ventricular pressure were measured indirectly by the model estimation method. The computer results show that the CIAPC system could maintain hemodynamic stability under extreme physiological conditions, effectively preventing ventricular suction and pump regurgitation. In a resting state, the system could automatically adjust and maintain personalized cardiac output (4 L/min, 5 L/min, and 7 L/min) based on patient body type differences, while ensuring that the cardiac index for all patients remains stable at around 3 L/min/m^2, which is within the normal physiological range. Furthermore, following an approximate 30 s period of transitional adjustment, the CIAPC system demonstrated the capacity to dynamically modulate cardiac output in response to patient needs. Specifically, it was able to increase the cardiac output of a patient with a normal body type from 5 L/min at rest to 8 L/min during exercise, or decrease it to 4 L/min during sleep. The CIAPC can control the rotary pump speed of the CFLVAD based on individual characteristics, enabling the delivery of personalized therapy to patients.

1. Introduction

Heart failure represents a significant global health concern, with an increasing prevalence observed annually (Molina et al., 2021). The continuous-flow Left ventricular assist device (CFLVAD) implantation is an effective treatment for end-stage heart failure and has replaced heart transplantation as the gold standard (Habigt et al., 2021; Mancini & Colombo, 2015). Despite the significant technological advances that have been made in CFLVADs, patient quality of life and adverse events remain important constraints to CFLVAD therapy (Kilic et al., 2023).

At present, CFLVADs operate at a constant speed, with pump speed manually set by a skilled clinician based on the patient's perfusion needs during a routine physical examination (Maw et al., 2022; Stephens, Busch, Salamonsen, Gregory, & Tansley, 2021). During CFLVAD therapy, a complex medical management system is employed to ensure patient comfort and safety. The pump speed is a key adjustment parameter in the management system (Belkin, Kagan, Labuhn, Pinney, & Grinstein, 2022). Studies have shown that CFLVADs operating at constant speed are insensitive to ventricular preload response compared to natural hearts, which are very sensitive to changes in preload (Bakouri & Sikkandar, 2020; Stephens et al., 2020). However, due to the lack of preload sensitivity, CFLVAD is unable to respond to the body's ever-changing physiological environment, which predisposes rotary pump to over-pumping or under-pumping and can also lead to adverse events

* Corresponding author.
E-mail addresses: liuhongtao0114@163.com (H. Liu), aili_guan@163.com (A. Guan), xingfayu@163.com (F. Xing), zhangyp@sdu.edu.cn (Y. Zhang), wwcwfu@126.com (W. Wang), pandalgx@126.com (G. Liu).
[1] These authors contributed equally to this work.

https://doi.org/10.1016/j.eswa.2025.128536
Received 16 August 2024; Received in revised form 14 May 2025; Accepted 6 June 2025
Available online 12 June 2025

and the development of complications (Tchantchaleishvili et al., 2017; Wu et al., 2020).

Physiologic control for CFLVAD attempts to improve the adaptivity of the pump by automatically adjusting the pump speed to pump the appropriate rotary pump flow in response to changes in the patient's physiologic state. Several system inputs have been proposed for adjusting pump speed, such as ventricular preload (Fetanat, Stevens, Hayward, & Lovell, 2020, 2021), pump speed difference (Meki et al., 2020; Wang, Koenig, Slaughter, & Giridharan, 2015), pump pressure difference (Gao, Chang, Gu, Zeng, & Liu, 2012), aortic pressure (Wu & Zheng, 2015), rotary pump flow (Bozkurt, van Tuijl, Schampaert, van de Vosse, & Rutten, 2014; Bozkurt, van Tuijl, van de Vosse, & Rutten, 2016), and heart rate (Jing, Xin, Wang, Zhang, & Zhou, 2022). In physiological control systems, these inputs are usually set to a fixed value that serve as a system reference. Nevertheless, the system inputs have been fixed and are unable to follow the physiological systems to implement real-time adjustments. Consequently, the control systems are deficient in their physiological dynamicity. Some research groups have proposed Starling-like control as a potential means of improving the physiological dynamicity of control systems. The Starling-like control can simulate the Frank-Starling mechanism inherent in the natural heart (Stephens et al., 2020; Stephens, Gregory, & Salamonsen, 2019b). This mechanism allows for improved CFLVAD sensitivity to ventricular preload and reduced CFLVAD sensitivity to ventricular afterload (Hildebrand et al., 2022). Consequently, Starling-like control can prevent the occurrence of adverse events such as ventricular suction and congestion (Pauls et al., 2016b; Stephens, Stevens, Gregory, Kleinheyer, & Salamonsen, 2017). The Starling-like control mechanism regulates pump speed and flow in real-time through dynamic ventricular preload, ensuring the patient's cardiac output is met (Ng et al., 2017; Stephens, Gregory, Tansley, Busch, & Salamonsen, 2019a). The ventricular preload variables adopted by the Starling-like controller included left ventricular end-diastolic pressure (Ng et al., 2018; Stephens et al., 2019a, 2021, 2017; Wang et al., 2022), left ventricular end-diastolic volume (Habigt et al., 2021; Ochsner et al., 2014), and left atrial pressure (Ng et al., 2017; Stephens et al., 2019b). However, a main limitation of Starling-like control, which relies on preload information in decision-making, is the absence of clinically implantable pressure or volume sensors.

Several physiological control strategies for CFLVAD have been proposed previously, of which Starling-like control is considered the most physiological initiative and application prospect (Stephens et al., 2020). The execution of the Starling-like controller depends on a functional relationship between cardiac output and ventricular preload. The cardiac output is used as the desired rotary pump flow . However, cardiac output in patients with CFLVAD does not significantly reflect interpatient variability (Tanner & Rhoades, 2003). For example, the normal cardiac output of a patient weighing 50 kg may differ from that of a patient weighing 70 kg. Consequently, cardiac output is not an optimal choice as a dynamic input to the control system. The cardiac index turns cardiac output into a normalized value that accounts for the heart rate and body size of the patient, thus better reflecting the patient's individual characteristics. In addition, heart rate is a physiological variable that responds to the physiological environment and can be detected from the body surface without the need to implant sensors. Building upon these considerations, this study introduces a cardiac index adaptive physiological control (CIAPC) strategy, a novel control approach designed to enhance CFLVAD personalized therapy. To establish the feasibility of CIAPC, we first performed a comparative analysis of cardiac output and cardiac index across patients with divergent body types, thereby validating its capacity to accommodate interpatient physiological variability. The safety of CIAPC was further evaluated under two extreme conditions, which was reflected in the ability to avert ventricular suction and pump regurgitation. Moreover, by designing daily transition scenarios, including rest to exercise and rest to sleep, we systematically investigated the robustness and physiological adaptability of the CIAPC strategy.

This paper is organized as follows: Section 2 introduces the design methodology for the CIAPC system, outlines the architecture of its components, and details the simulation protocol. Section 3 provides an analysis of individual differences, performance assessments under extreme conditions, and evaluations of dynamic responses during transitions in daily scenarios. In Section 4, a comparative analysis of the heart index and cardiac output as control parameters is presented, followed by a discussion that contrasts existing research across three dimensions: measurement feedback, pump regurgitation, and scenario simulation. Additionally, the limitations of this study are described in Section 4. Finally, Section 5 presents the conclusions drawn from the findings of this research.

2. Methods

2.1. Cardiovascular coupled system model

The CIAPC system was constructed based on the cardiovascular coupling system model (Fig. 1) previously developed by our group. The cardiovascular coupling system model consists of three parts: the cardiovascular system model, the baroreflex model, and the CFLVAD model. Further details on the cardiovascular coupling system model can be found in Liu, Liu, Ma, and Zhang (2020), Liu, Liu, and Ma (2021).

The cardiovascular system model was constructed using the lumped parameter unit, which divided the circulatory system into distinct sections that included the left heart, right heart, systemic circulation, and pulmonary circulation. Each section consisted of several lumped parameter blocks with hemodynamic factors such as resistance, compliance, pressure, and flow. The ideal elements resistor, capacitor, inductor, and diode were used to characterize the blocks of lumped parameters. Furthermore, Kirchhoff's law was utilized to describe the relationship between hemodynamic factors.

The baroreflex model was used to simulate the neural regulation of aortic pressure, with the aim of regulating left ventricular end-systolic elastance, right ventricular end-systolic elastance, systemic vascular resistance, and heart rate in the cardiovascular system model.

The CFLVAD model developed by Choi, Boston, Thomas, and Anta (1997) and Pillay and Krishnan (1989) was adopted to simulate the dynamics of the rotary pump and to test the proposed CIAPC strategy. The CFLVAD model includes a mechanical dynamics model and a hydrodynamic characteristics model, as shown in Eqs. (1) and (2), respectively.

$$J\frac{d\omega}{dt} = \frac{3}{2}K_B I - B\omega - a_0\omega^3 - a_1 Q_{rp}\omega^2 \tag{1}$$

$$H = b_0 Q_{rp} + b_1\frac{dQ_{rp}}{dt} + b_2\omega^2 \tag{2}$$

where J is the rotor inertia, ω is pump speed in rpm (revolutions per minute), K_B is the back electromotive force constant, I is the phase current, B is the damping coefficient, a_0 and a_1 are correlation constants, Q_{rp} is the rotary pump flow in mL/s, H is the pump pressure difference, and b_0, b_1 and b_2 are experimental constants. The assigned values of the CFLVAD model parameters are listed in Table 1.

Table 1
CFLVAD model parameters (Liang et al., 2020).

Parameter	Value	Unit
J	9.16×10^{-7}	$Kg\cdot m^2$
K_B	0.003	$Kg\cdot m^2\cdot A^{-1}\cdot s^{-2}$
B	6.6×10^{-7}	$Kg\cdot m^2\cdot s^{-1}$
a_0	7.38×10^{-13}	$Kg\cdot m^2\cdot s\cdot mL^{-3}$
a_1	1.98×10^{-11}	$Kg\cdot m^2\cdot s\cdot mL$
b_0	−0.296	$mmHg\cdot s\cdot mL^{-1}$
b_1	−0.027	$mmHg\cdot s^2\cdot mL^{-1}$
b_2	9.33×10^{-5}	$mmHg\cdot s^2$

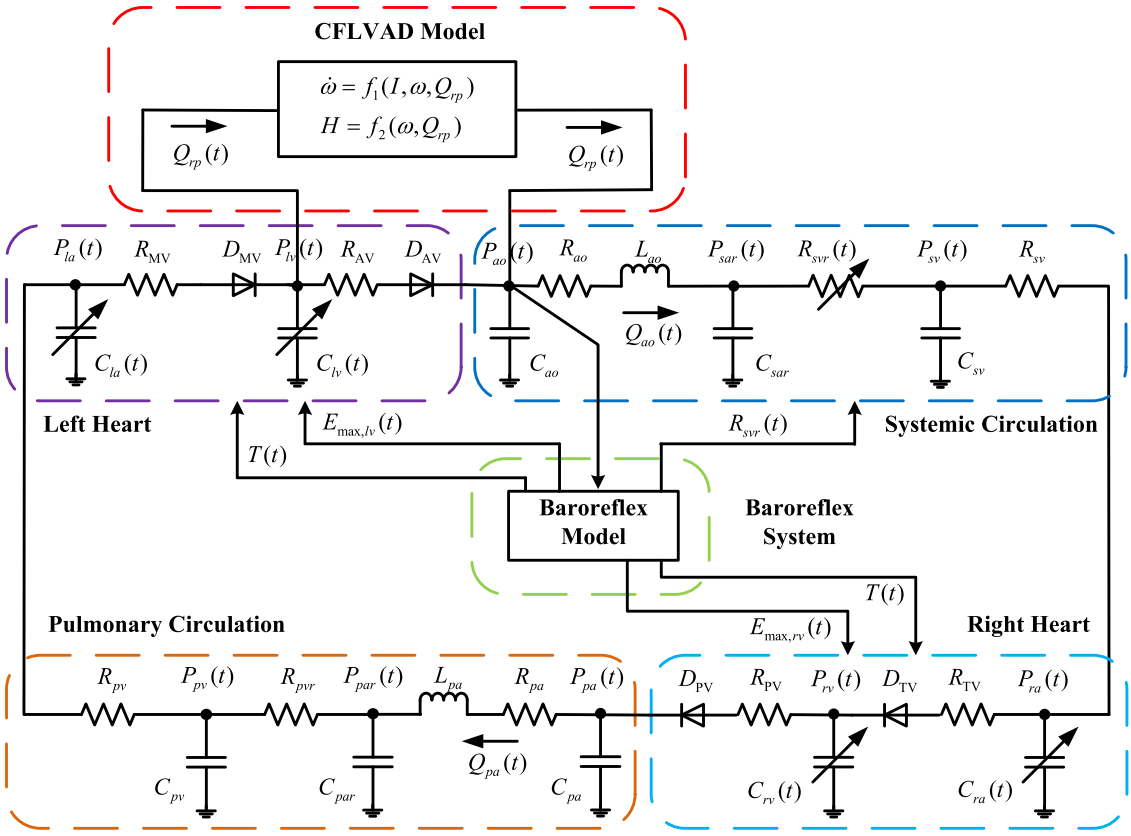

Fig. 1. Schematic representation of the cardiovascular coupling system model, which consists of a cardiovascular system model, a baroreflex model, and a CFLVAD model.

2.2. CIAPC system

Fig. 2 depicts the CIAPC system for CFLVAD. The cardiac index adaptive controller consists of the cardiac index regulator and the Fuzzy + ventricular suction prevention (VSP) controller. The execution of the cardiac index regulator is contingent upon a functional relationship between the cardiac index and the patient's body surface area (BSA), as well as the heart rate. The desired cardiac index output by the cardiac index regulator is compared to the feedback cardiac index quantified by the average rotary pump flow . The resulting error and the change of error are then fed into the Fuzzy + VSP controller, which is a combination of the Fuzzy controller and the VSP controller. The Fuzzy + VSP controller outputs the phase current, thereby regulating the pump speed and consequently the rotary pump flow . This results in the rotary pump flow being adjusted in real time to meet the physiological perfusion requirements of the cardiovascular system. The left ventricular pressure and rotary pump flow signals are measured indirectly using the model estimation method, whereas the aortic pressure and heart rate

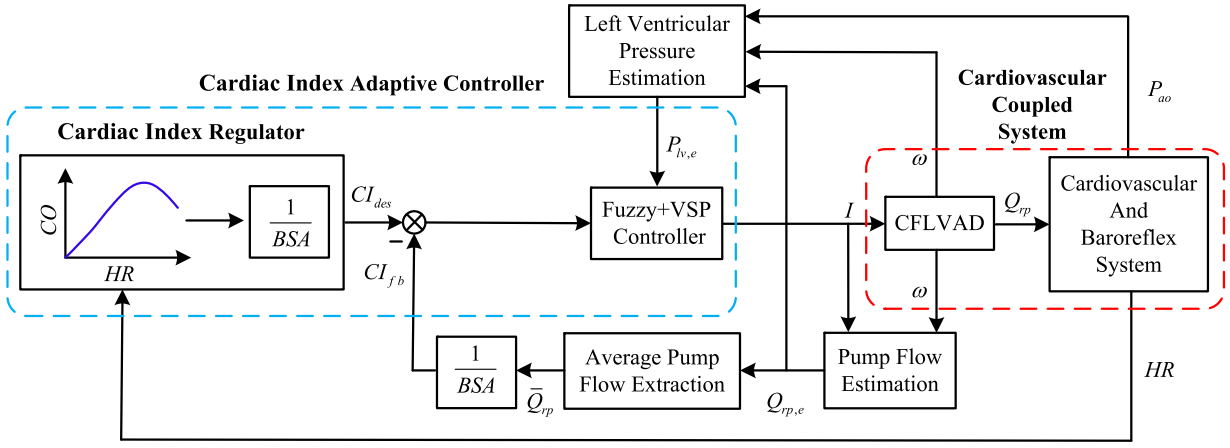

Fig. 2. CIAPC system for CFLVAD. CO represents the cardiac output, HR represents the heart rate, P_{ao} represents the aortic pressure, BSA represents the body surface area, CI_{des} is the desired cardiac index, CI_{fb} is the feedback cardiac index, $Q_{rp,e}$ is the model-estimated rotary pump flow , $\bar{Q}_{rp}$ is the average rotary pump flow after model estimation, Q_{rp} is the rotary pump flow from the CFLVAD output, $P_{lv,e}$ is the model-estimated left ventricular pressure, I is the phase current, ω is the pump speed, and VSP is an abbreviation for ventricular suction prevention. In the control system, the error between CI_{des} and CI_{fb}, along with the change of error, as inputs for the Fuzzy + VSP controller. Additionally, the nonlinear relationship between CO and HR is depicted by the blue curve.

signals can be detected using sensors from the body surface. Thus, the cardiac index adaptive controller can be performed without having to resort to implantable sensors.

2.2.1. Cardiac index regulator

The cardiac index regulator describes the functional relationship that exists between the desired cardiac index and the individual characteristics (BSA and heart rate). The BSA is related to the patient's height and weight. However, there is no direct relationship between cardiac index and heart rate as well as the patient's height and weight. Therefore, formulaic reasoning is required to set up the functional equation.

Cardiac output is calculated as the product of stroke volume and heart rate, as shown in Eq. (3).

$$CO = SV \cdot HR \tag{3}$$

where CO is the cardiac output, SV is the ventricular stroke volume, and HR is the heart rate.

Eq. (4) expresses the functional relationship between left ventricular stroke volume and cardiac cycle (Jing et al., 2022).

$$SV = \frac{f \cdot T \cdot T_s}{T - T_s} \tag{4}$$

where T_s is the left ventricular systolic period, T is the cardiac cycle, and f is the coefficient with a value of 0.162 min /L.

The relationship between heart rate and cardiac cycle is shown in Eq. (5).

$$HR = \frac{60}{T} \tag{5}$$

Eqs. (4) and (5) are substituted into Eq. (3) to yield

$$CO = \frac{60 f T_s}{T - T_s} \tag{6}$$

The linear equation between left ventricular systole period and heart rate (Weissler, Harris, & Schoenfeld, 1968):

$$T_s = u \cdot HR + v \tag{7}$$

where u and v represent the coefficients of the linear equation, with values of –0.001 s^2 and 0.36 s, respectively.

Substituting Eqs. (5) and (7) into Eq. (6) gives the nonlinear equation between cardiac output and heart rate as follows:

$$CO = \frac{60 f (uHR^2 + vHR)}{60 - uHR^2 - vHR} \tag{8}$$

The BSA is calculated using the following formula (Yu, Lin, & Yang, 2010):

$$BSA = 7.13989 \times 10^{-3} H^{0.7437} W^{0.404} \tag{9}$$

where BSA is the body surface area in m^2, H is the stature height in cm, and W is the body weight in kg.

The formula for calculating the cardiac index is

$$CI = \frac{CO}{BSA} \tag{10}$$

where CI is the cardiac index.

Eqs. (8) and (9) are substituted into Eq. (10) to obtain expressions for the desired cardiac index as a function of heart rate, height, and weight:

$$CI_{des} = \frac{60 f (uHR^2 + vHR)}{(60 - uHR^2 - vHR)(7.13989 \times 10^{-3} H^{0.7437} W^{0.404})} \tag{11}$$

where CI_{des} is the desired cardiac index output by the cardiac index regulator.

2.2.2. Estimation of rotary pump flow and left ventricular pressure

The current and speed of the motor are measured and used as inputs to Eq. (1), which represents the mechanical dynamics model of the rotating pump. This allows the model-estimated rotary pump flow ($Q_{rp,e}$) to be derived.

$$Q_{rp,e} = \frac{\frac{3}{2} K_B I - B\omega - a_0\omega^3 - J\frac{d\omega}{dt}}{a_1\omega^2} \tag{12}$$

As shown in Fig. 1, the rotary pump bridges the aorta and left ventricle. Consequently, the pump pressure difference is the difference between the aortic pressure and the left ventricular pressure. The model-estimated left ventricular pressure is derived by substituting the aortic pressure, pump velocity, and model-estimated rotary pump flow into Eq. (2), which is expressed by Eq. (13).

$$P_{lv,e} = P_{ao} - b_0 Q_{rp,e} - b_1 \frac{dQ_{rp,e}}{dt} - b_2\omega^2 \tag{13}$$

where P_{ao} is the aortic pressure that can be detected from the body surface.

2.2.3. Feature extraction

The average rotary pump flow and left ventricular systolic pressure are extracted from the data set of model-estimated rotary pump flow and left ventricular systolic pressure during a cardiac cycle. The equations for average rotary pump flow and left ventricular systolic pressure at the kth cardiac cycle are listed below.

$$\bar{Q}_{rp}(k) = \frac{\sum_{i=1}^{n(k)} Q_{rp,e}(k,i)}{n(k)} \tag{14}$$

$$P_{lv,sys}(k) = \max_{1 \le i \le n(k)} (P_{lv,e}(k,i)) \tag{15}$$

$$n(k) = \frac{60 f_s}{HR(k)} \tag{16}$$

where $\bar{Q}_{rp}(k)$ is the average rotary pump flow at the kth cardiac cycle, $P_{lv,sys}(k)$ is the left ventricular systolic pressure at the kth cardiac cycle, $Q_{rp,e}(k,i)$ is the ith sampling value in the sampling set of model-estimated rotary pump flow during the kth cardiac cycle, $P_{lv,e}(k,i)$ is the ith sampling value in the sampling set of model-estimated left ventricular during the kth cardiac cycle, $n(k)$ is the number of samples corresponding to the kth cardiac cycle, $HR(k)$ is the heart rate corresponding to the kth cardiac cycle, and f_s is the sampling frequency with a value of 1000 Hz.

2.2.4. Fuzzy + VSP controller

The Fuzzy + VSP controller consists of the Fuzzy controller and the VSP controller. The execution flow of these controllers is shown in Fig. 3. The system initiates the process by initializing the cardiac cycle counter ($k = 1$) and the motor phase current $I(k)$, while monitoring the left ventricular systolic pressure $P_{lv,sys}(k)$ throughout the current cardiac cycle. When $P_{lv,sys}(k)$ exceeds a threshold of 20 mmHg, the system automatically activates the Fuzzy Controller, which employs fuzzy logic algorithms to determine the optimal current adjustment $\Delta I(k)$. This adjustment is subsequently applied to update the current for the subsequent cardiac cycle through an incremental adjustment strategy defined as $I(k+1) = I(k) + \Delta I(k)$. Conversely, if $P_{lv,sys}(k)$ falls below 20 mmHg, the system transitions to the VSP controller to prevent excessive unloading of the ventricle. In this case, the current output is reduced by a predetermined safety decay coefficient C, represented as $I(k+1) = I(k) - C$. After each cardiac cycle, the system updates $I(k)$ and increments k, thereby establishing a closed-loop feedback control system that responds in real time to fluctuations in left ventricular pressure. This control mechanism ensures that the CFLVAD can dynamically adjust its output following actual physiological demands, thereby maintaining adequate blood flow perfusion while minimizing the risk of excessive ventricular unloading.

The VSP controller was designed to prevent the over-pumping of rotary pump under extreme conditions where over-pumping can result in excessive ventricular unloading or ventricular suction. The VSP controller operates by established physiological principles. The normal systolic pressure of the right ventricle is typically maintained within the range of 15–25 mmHg, with a mean value of approximately 20 mmHg. Clinical studies suggest that during CFLVAD support, maintaining a neutral interventricular septum position by an appropriate pressure gradient between the left and right ventricles can prevent suction (Dual,

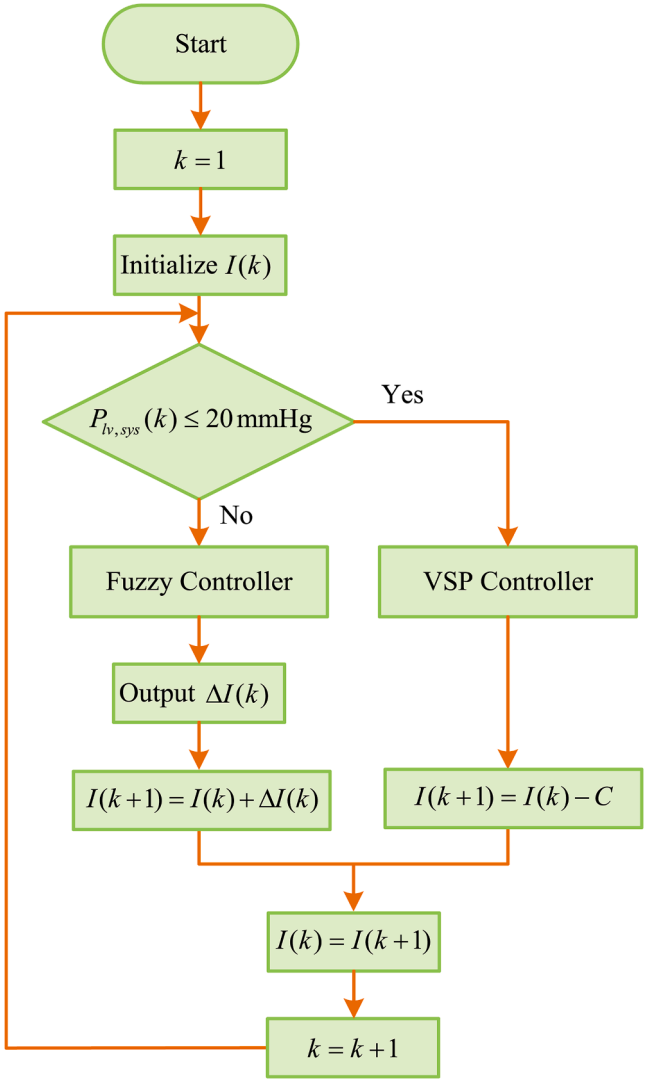

Fig. 3. Fuzzy + VSP controller execution flowchart. $P_{lv,sys}(k)$ is the left ventricular systolic pressure at the kth cardiac cycle, $I(k)$ or $I(k+1)$ denotes the motor phase current output by the Fuzzy + VSP controller at the $k\,th$ or $(k+1)th$ cardiac cycle, $\Delta I(k)$ is the change in the output current of the Fuzzy controller, and C represents a constant that indicates the reduced current during a single cardiac cycle within the framework of the VSP controller.

Anthamatten, Shah, Meboldt, & Schmid Daners, 2020). A decrease in $P_{lv,sys}$ below the safety threshold of 20 mmHg may signify a potential abnormal displacement of the interventricular septum towards the left ventricle, serving as an early warning indicator for ventricular suction and reflecting excessive pumping by the CFLVAD. To mitigate this risk, the control system incorporates a dynamic adjustment mechanism: if $P_{lv,sys}$ is less than or equal to 20 mmHg during the kth cardiac cycle, the current is subsequently reduced in the $(k+1)th$ cardiac cycle by Eq. (17).

$$I(k+1) = I(k) - C \tag{17}$$

where C is a constant that represents the attenuation of current during a single cardiac cycle, with a value of 0.02 A.

The input to the Fuzzy controller is the error between the desired cardiac index CI_{des} and the feedback cardiac index CI_{fb} and the change of error δE. The output of the Fuzzy controller is the current change. Here, the feedback cardiac index is the ratio of average rotary pump flow to BSA, as shown in Eq. (18).

$$CI_{fb} = \frac{\bar{Q}_{rp}}{BSA} \tag{18}$$

where CI_{fb} is the feedback cardiac index.

Table 2
The rules for fuzzy controller.

ΔI		δE						
		NB	NM	NS	Z	PS	PM	PB
E	NB	NB	NB	NB	NB	NM	Z	Z
	NM	NB	NB	NB	NB	NM	Z	Z
	NS	NM	NM	NM	NM	Z	PS	PS
	Z	NM	NM	NS	Z	PS	PM	PM
	PS	NS	NS	Z	PM	PM	PM	PM
	PM	Z	Z	PM	PB	PB	PB	PB
	PB	Z	Z	PM	PB	PB	PB	PB

The input error of the Fuzzy controller at the kth cardiac cycle is defined as

$$E(k) = CI_{des} - CI_{fb} \tag{19}$$

and the change of error is defined as

$$\delta E(k) = E(k) - E(k-1) \tag{20}$$

The change in the output current of the Fuzzy controller is represented by $\Delta I(k)$. After Fuzzy controller processing, the current of the next cardiac cycle is updated to

$$I(k+1) = I(k) + \Delta I(k) \tag{21}$$

The fuzzy controller internally performs three operations: fuzzification of inputs, fuzzy inference based on control rules, and defuzzification to obtain a clear value for the control signal. In the fuzzification design, the triangular and trapezoidal membership functions were used to define the fuzzy sets for E , δE , and ΔI (Fig. 4), where “large negative” (NB), “medium negative” (NM), “ “small negative” (NS), “zero” (Z), “small positive” (PS), “medium positive” (PM) and “large positive” (PB) are the linguistic labels. Table 2 lists the fuzzy inference rules for the fuzzy controller. Finally, the centroid method was used to complete the defuzzification.

2.3. Simulation protocol

A number of parameters in the cardiovascular and baroreflex system model were adjusted (Table 3) to simulate scenarios of patients in their daily lives including rest, exercise, and sleep. In this study, the parameters in the rest scenario were used as a baseline for configuring the parameters in the exercise and sleep scenarios. This was achieved by increasing or decreasing parameters related to HR , left ventricular end-systolic elastance ($E_{\max,lv}$), right ventricular end-systolic elastance ($E_{\max,rv}$), systemic vascular resistance (R_{svr}), and pulmonary vascular resistance (R_{pvr}). This approach is analogous to the parameter configurations used by Stephens et al. (2019a) and Pauls et al. (2016a) in their CFLVAD physiological control studies. A detailed description of the parameters associated with Table 3 can be found in Liu et al. (2020).

The height/weight of patients with thin, normal, and obese body types was assumed to be 160 cm/45 kg, 170 cm/55 kg, and 180 cm/105 kg, respectively. CO and CI were compared in patients with different body types at rest. In this study, CO is the sum of rotary pump flow and left ventricular output flow, i.e., aortic flow.

Take the patient with normal body type for example, the performances of CIAPC in preventing ventricular suction and pump regurgitation were tested by step change in ventricular preload and afterload to create two extreme physiological conditions. First, a sharp reduction in left ventricular flow was simulated by increasing left ventricular preload resistance, i.e., R_{pvr} and decreasing left ventricular afterload resistance , i.e., R_{svr}. This extreme condition was established to test the performance of CIAPC in preventing ventricular suction. Second, a sharp increase in left ventricular flow was simulated by decreasing R_{pvr} and increasing R_{svr}. This extreme condition was established to test the performance of CIAPC in preventing pump regurgitation. Although there is no step

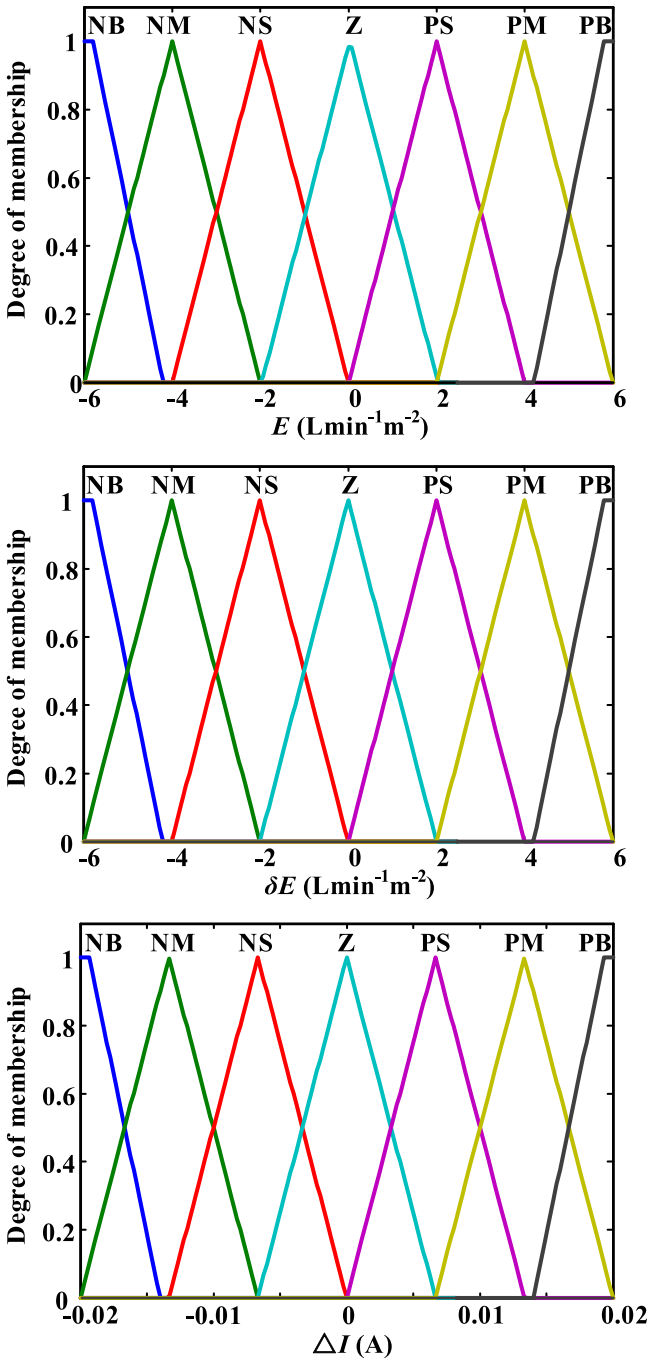

Fig. 4. Membership functions used to determine the change in phase current.

change in the physiological system, the step disturbance can harshly test the robustness of the control system. Therefore, if CIAPC can respond well enough to physiological disturbances for these extreme conditions, it can also respond appropriately to mild disturbances. Also, the left ventricular suction was defined as a left ventricular end-diastolic pressure of less than 0 mmHg, and the pump regurgitation was defined as the minimum rotary pump flow of less than 0 mL/s.

Take the patient with normal body type for example, the adaptive performance of CIAPC was evaluated by the responses to I, ω, CO, CI, blood pressure and left ventricular volume (V_{lv}) in the rest-sleep-rest and rest-exercise-rest scenarios. Transitions between sleep and rest, as well as between rest and exercise, were simulated by using the ramp function to represent the changes in the physiological variables in Table 3.

Table 3
Parameters associated with heart rate (HR), left ventricular end-systolic elastance ($E_{\max,lv}$), right ventricular end-systolic elastance ($E_{\max,rv}$), systemic vascular resistance (R_{svr}), and pulmonary vascular resistance (R_{pvr}) in the cardiovascular and baroreflex system are adjusted to simulate the patients' daily activity scenarios.

Scenario	Physiological variable	Associated parameter	Value	Unit
Rest (Baseline)	HR	T_0	0.52	s
		G_{T_s}	−0.08	$s^2 \cdot spikes^{-1}$
		G_{T_v}	0.07	s^2/spikes
	$E_{\max,lv}$	$E_{\max,lv0}$	0.14	mmHg/mL
		$G_{E_{\max,lv}}$	0.275	mmHg · s/mL/spikes
	$E_{\max,rv}$	$E_{\max,rv0}$	0.65	mmHg/mL
		$G_{E_{\max,rv}}$	0.275	mmHg · s · mL/spikes
	R_{svr}	R_{svr0}	0.74	mmHg · s/mL
		$G_{R_{svr}}$	0.33	mmHg · s/mL/spikes
	R_{pvr}	–	0.12	mmHg · s/mL
Sleep	$HR\downarrow$	T_0	0.51	s
		G_{T_s}	−0.04	$s^2 \cdot spikes^{-1}$
		G_{T_v}	0.16	s^2/spikes
	$E_{\max,lv}\downarrow$	$E_{\max,lv0}$	0.07	mmHg/mL
		$G_{E_{\max,lv}}$	0.105	mmHg · s/mL/spikes
	$E_{\max,rv}\downarrow$	$E_{\max,rv0}$	0.38	mmHg/mL
		$G_{E_{\max,rv}}$	0.205	mmHg · s · mL/spikes
	$R_{svr}\downarrow$	R_{svr0}	0.42	mmHg · s/mL
		$G_{R_{svr}}$	0.23	mmHg · s/mL/spikes
	R_{pvr}	–	0.12	mmHg · s/mL
Exercise	$HR\uparrow$	T_0	0.38	s
		G_{T_s}	−0.07	$s^2 \cdot spikes^{-1}$
		G_{T_v}	0.04	s^2/spikes
	$E_{\max,lv}\uparrow$	$E_{\max,lv0}$	0.16	mmHg/mL
		$G_{E_{\max,lv}}$	0.305	mmHg · s/mL/spikes
	$E_{\max,rv}\uparrow$	$E_{\max,rv0}$	0.85	mmHg/mL
		$G_{E_{\max,rv}}$	0.305	mmHg · s · mL/spikes
	$R_{svr}\downarrow$	R_{svr0}	0.54	mmHg · s/mL
		$G_{R_{svr}}$	0.11	mmHg · s/mL/spikes
	$R_{pvr}\downarrow$	–	0.07	mmHg · s/mL

The symbol "↑" indicates that the current physiological variable has increased from the baseline physiological variable, while the symbol "↓" indicates that the current physiological variable has decreased from the baseline physiological variable.

3. Results

3.1. Individual difference

Table 4 lists the cardiac output and cardiac index provided by the CIAPC at rest for patients of all three body types. CIAPC provides differential cardiac output for patients with different BSA. CIAPC provided approximately 4 L/min cardiac output for thin patients with a BSA of 1.45 m^2 and approximately 7 L/min for obese patients with a BSA of 2.23 m^2. The CIAPC provides a differentiated cardiac output that is customized for patients according to their BSA. This methodology guarantees that patients maintain a normal cardiac index of approximately 3 L/min/m^2 while at rest, thereby meeting standard metabolic demands and avoiding the risks associated with both under-pumping and over-pumping in rotary pumps.

Table 4
Cardiac output (CO) and cardiac index (CI) provided by CIAPC at rest for patients of all three body types.

Patient characteristic			Cardiac function indicators	
H (cm)	W (Kg)	BSA (m^2)	CO (L/min)	CI (L/min/m^2)
160	45	1.45	4.32	2.99
170	55	1.64	5.03	3.06
180	105	2.23	7.06	3.17

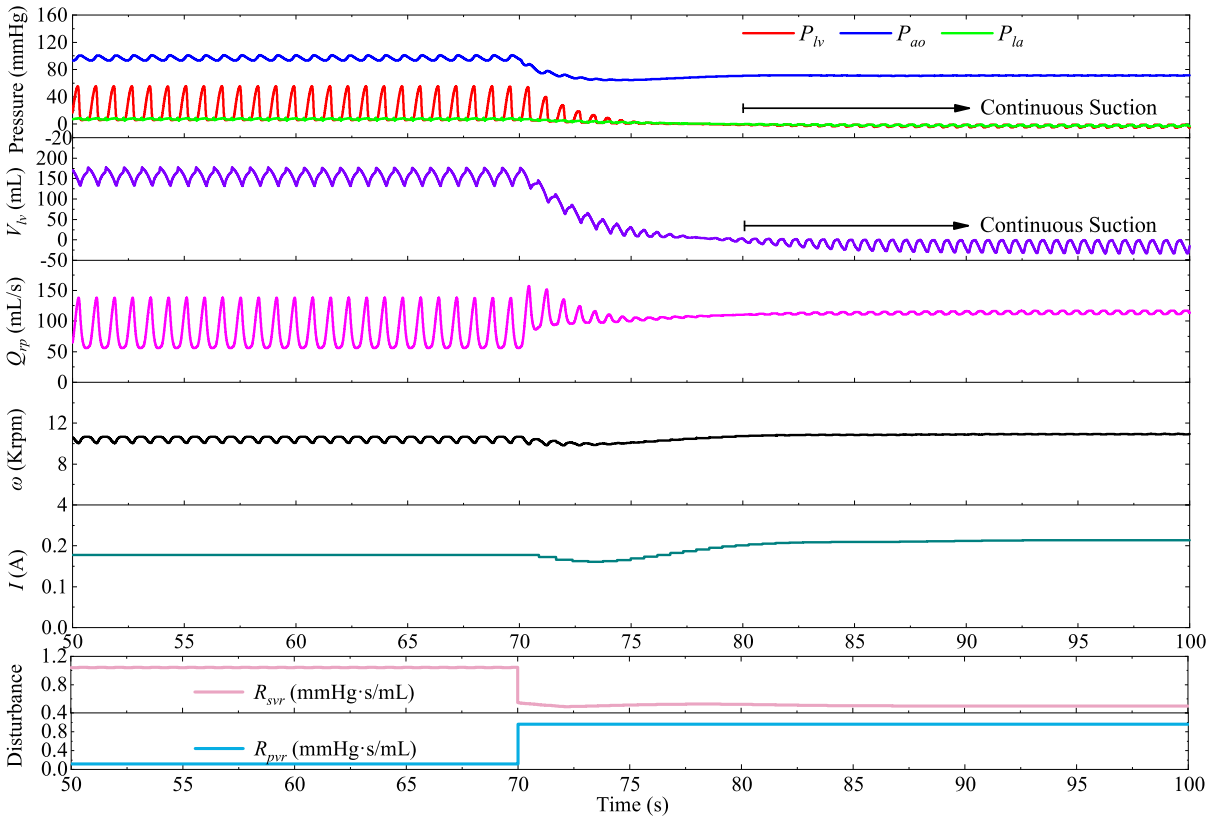

Fig. 5. System responses when CIAPC is without VSP controller to address a sharp decrease in left ventricular flow. P_{lv} is the left ventricular pressure, P_{la} is the left atrial pressure, P_{ao} is the aortic pressure, V_{lv} is the left ventricular volume, Q_{rp} is the rotary pump flow , ω is the pump speed, I is the current, R_{pvr} is the left ventricular preload resistance, and R_{svr} is the left ventricular afterload resistance.

3.2. Performance for ventricular suction prevention

The system responses when the CIAPC is without and with the VSP controller are shown in Figs. 5 and 6, respectively. Figs. 5 and 6 show a step change in R_{pvr} from 0.12 mmHg · s/mL to 0.96 mmHg · s/mL and a step change in R_{svr} from 1 mmHg · s/mL to 0.5 mmHg · s/mL at the 70th s. These changes were designed to simulate an extreme condition in which left ventricular flow is sharply reduced. When the CIAPC was without the VSP controller, the end diastolic pressure and volume of the left ventricular were below 0 since the 80th s, indicating the presence of continuous suction (Fig. 5). When the CIAPC was equipped with a VSP controller, the system exhibited a smooth transition between 70 and 80 s in response to pressure, volume, and flow. After 10 s, I and ω were adjusted in real time to avoid ventricular suction (Fig. 6).

3.3. Performance for pump regurgitation prevention

Fig. 7 depicts the system responses when CIAPC addressed a sharp increase in left ventricular flow. At the 70th s, there was a step change in R_{pvr} from 0.12 mmHg · s/mL to 0.04 mmHg · s/mL and a step change in R_{svr} from 1 mmHg · s/mL to 1.3 mmHg · s/mL. These changes were designed to simulate an extreme condition in which left ventricular flow is sharply increased. From the onset of the physiological disturbance at the 70th s, CIAPC continuously controlled the I to modulate the ω and Q_{rp}. After about 10 s, the hemodynamic parameters in the cardiovascular system, including left ventricular pressure (P_{lv}), left atrial pressure (P_{la}), aortic pressure (P_{ao}), and left ventricular volume (V_{lv}), reached a steady state. The rotary pump flow curve shows that the Q_{rp} was always greater than 0 mL/s as the system changes from the steady state before the 70th s to the transient state after the 70th s and then to the new steady state.

3.4. Simulation for rest-exercise-rest scenario

Fig. 8 shows the system responses for CIAPC as the patient transitions from a rest state to an exercise state and then back to a rest state. The left ventricular end-systolic elastance ($E_{\max,lv}$), right ventricular end-systolic elastance ($E_{\max,rv}$), and HR slope increased approximately between 1.6 and 2 min, while R_{pvr} and R_{svr} slope decreased, thus simulating the transition from rest to exercise. During the transition from rest to exercise, the cardiac index adaptive controller maintains a continuous increase in I to enhance ω and Q_{rp}. $E_{\max,lv}$, $E_{\max,rv}$, and HR slope decreased between 3.8 and 4.2 min, while R_{pvr} and R_{svr} slope increased, thus simulating the transition from exercise to rest. During the transition from exercise to rest, the cardiac index adaptive controller maintains a continuous decrease in I to diminish ω and Q_{rp}. Compared to the rest state, P_{lv} and V_{lv} decreased in the exercise state, while P_{ao} and P_{la} hardly changed. Additionally, HR increased from 75 beats per minute (bpm) at rest to about 120 bpm during exercise. Similarly, CO rose from 5 L/min at rest to 8 L/min at exercise. During the patient's activity transition, CI_{des} undergoes continuous change in response to the physiological disturbance. Through CIAPC, CI_{fb} is able to quickly and accurately track CI_{des}. An increase in cardiac index was observed from 3.06 L/min/m^2 at rest to 4.88 L/min/m^2 at exercise.

3.5. Simulation for rest-sleep-rest scenario

Fig. 9 shows the system responses for CIAPC as the patient transitions from a rest state to a sleep state and then back to a rest state. $E_{\max,lv}$, $E_{\max,rv}$, HR, and R_{svr} slope decreased approximately between 1.6 and 2

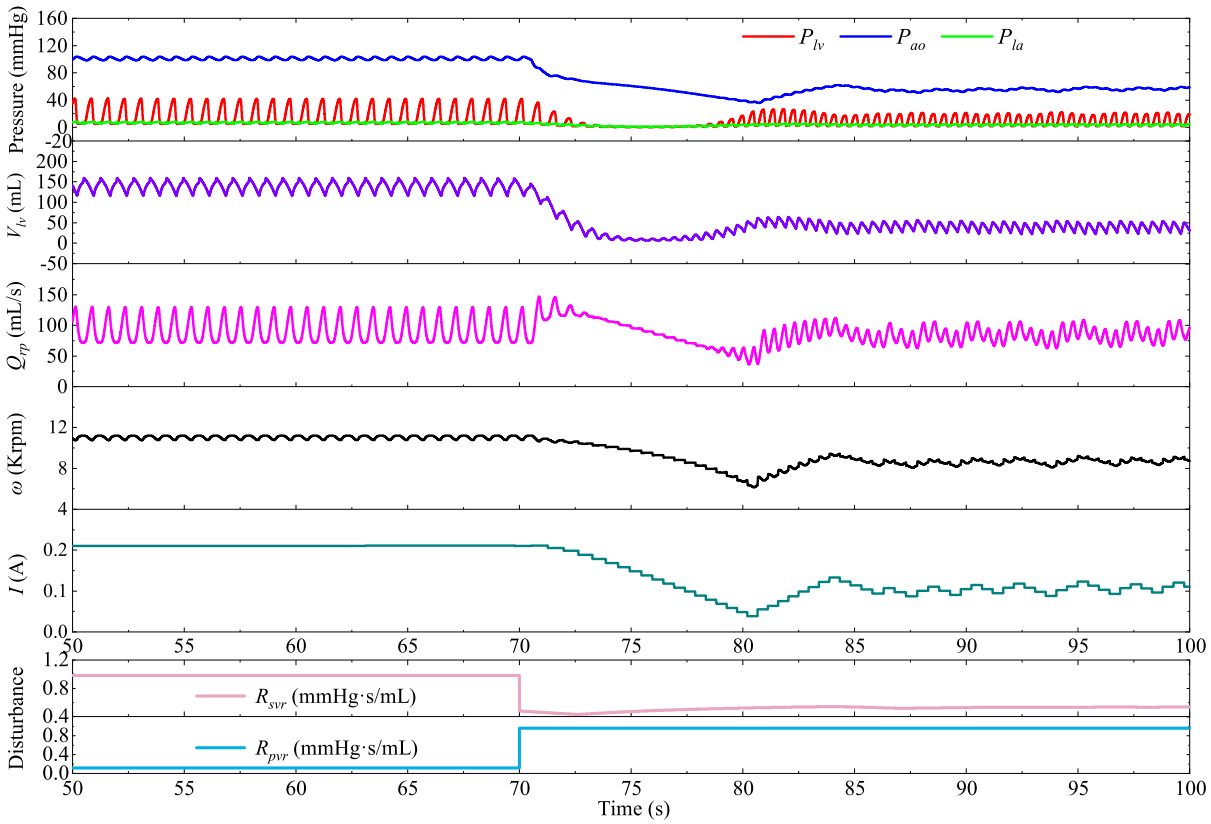

Fig. 6. System responses when CIAPC is with VSP controller to address a sharp decrease in left ventricular flow. P_{lv} is the left ventricular pressure, P_{la} is the left atrial pressure, P_{ao} is the aortic pressure, V_{lv} is the left ventricular volume, Q_{rp} is the rotary pump flow , ω is the pump speed, I is the current, R_{pvr} is the left ventricular preload resistance, and R_{svr} is the left ventricular afterload resistance.

min, thus simulating the transition from rest to sleep. During the transition from rest to sleep, the cardiac index adaptive controller maintains a continuous decrease in I to diminish ω and Q_{rp}. $E_{\max,lv}$, $E_{\max,rv}$, HR, and R_{svr} slope increased between 3.8 and 4.2 min, thus simulating the transition from sleep to rest. During the transition from exercise to rest, the cardiac index adaptive controller maintains a continuous increase in I to enhance ω and Q_{rp}. Compared to rest, during sleep, V_{lv} and P_{la} increased, while P_{ao} decreased and P_{lv} hardly changed. Also, the HR decreased from 75 bpm at rest to about 60 bpm during sleep. Similarly, CO fell from 5 L/min at rest to 4 L/min at sleep. As the patient transitions from rest to sleep or from sleep to rest, CI_{des} changed continuously according to the physiological disturbance. The adaptive cardiac index controller continuously adjusted I so that CI_{fb} could quickly and accurately track CI_{des}. A decrease in cardiac index was observed from 3.06 L/min/m^2 at rest to 2.44 L/min/m^2 at sleep.

4. Discussion

In this study, the CIAPC strategy is proposed to personalize CFLVAD therapy. The novelty for CIAPC is to select a control system input, the cardiac index, which establishes an association between CFLVAD physiological control and individual characteristics through heart rate and BSA. The simulation results *in silico* demonstrate that CIAPC could provide differentiated cardiac output for individuals with different characteristics. Furthermore, CIAPC was able to cope with physiological disturbances under extreme conditions to prevent ventricular suction and pump regurgitation. The CIAPC adjusted the pump speed in real time according to the individual's activity state to meet the physiological perfusion needs. Physiological signals could be measured and fedbacked without implanted sensors in the CFLVAD physiological control system based on CIAPC.

In previous studies on CFLVAD physiological control, cardiac output was typically considered the primary objective for evaluating whether CFLVAD was adapted to physiological perfusion demands (Petrou, Monn, Meboldt, & Daners, 2017; Wu, Allaire, Tao, & Olsen, 2007). In CFLVAD patients, cardiac output is usually a standardized common index. For example, the cardiac output for a normal adult at rest is approximately 5 L/min. However, it should be noted that there are individual differences between patients, particularly with regard to the required cardiac output in patients with significant differences in body size. Consequently, this study used cardiac index as a quantitative index of CFLVAD physiological control, thus providing different cardiac output for patients with different characteristics (Table 4).

The Starling-like control system was developed to mimic the Frank-Starling mechanism in the human body (Stephens et al., 2019b). The Starling-like physiological control system improves the CFLVAD's sensitivity to ventricular preload. For example, if the ventricular preload drops to 0 mmHg, the rotary pump flow decreases to 0 L/min, effectively preventing ventricular suction (Stephens et al., 2021, 2020). Starling-like physiological control relies on ventricular preload to make decisions. Preload signals require the use of pressure or volume sensors for measurement and feedback. However, there are currently no commercially available pressure or volume sensors for CFLVADs, and implantation of sensors may increase the risk of postoperative complications such as thrombosis (Stephens et al., 2020). Therefore, the major limitation of Starling-like control is the lack of available biosensors. With this in mind, this study indirectly measured rotary pump flow and left ventricular pressure using a model estimated method and designed the cardiac index regulator depending on heart rate, thereby avoiding the use of implantable sensors. However, without considering changes in left ventricular pressure, the responds for CFLVAD physiological control system showed a continuous suction phenomenon

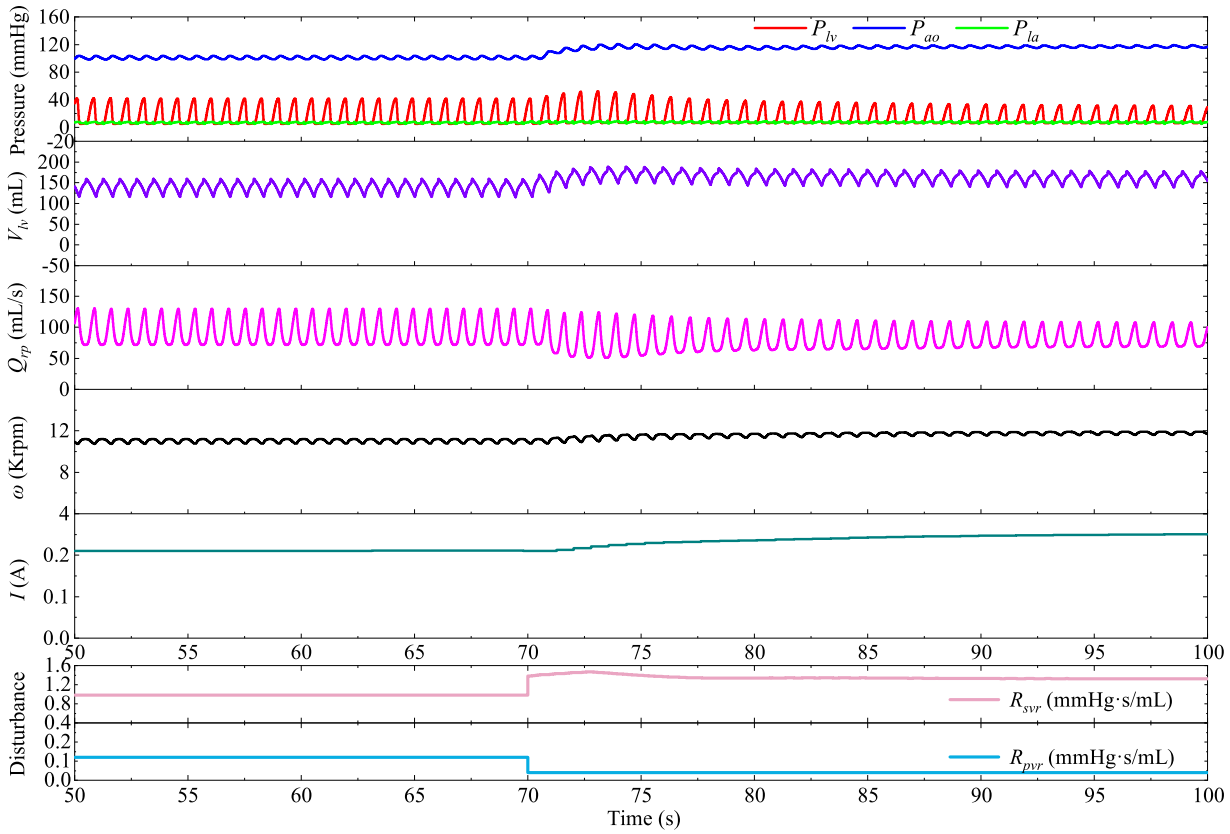

Fig. 7. Figure 7 System responses when CIAPC addresses a sharp increase in left ventricular flow. P_{lv} is the left ventricular pressure, P_{la} is the left atrial pressure, P_{ao} is the aortic pressure, V_{lv} is the left ventricular volume, Q_{rp} is the rotary pump flow , ω is the pump speed, I is the current, R_{pvr} is the left ventricular preload resistance, and R_{svr} is the left ventricular afterload resistance.

under extreme condition (Fig. 5). To make CFLVAD physiological control more sensitive to ventricular preload like Starling-like control, this study designed a VSP controller based on estimated left ventricular pressure, which effectively prevented ventricular suction under extreme condition (Fig. 6).

Despite the absence of physiological feedback in the CFLVAD constant speed control system, patients can be reassured that pump regurgitation is not a concern. This is due to the fact that the constant pump speed is the optimal safe speed as determined by the doctor. The pump outlet pressure corresponding to the constant speed is higher than the aortic pressure, so blood flow does not return from the aorta through the pump body to the left ventricle (Belkin et al., 2022). To improve the pulsatility of blood flow, some pulse modulation algorithms with the property of periodically increasing or decreasing the pump speed have been proposed. These pulse modulation algorithms have been shown to be prone to intermittent pump regurgitation if the pump speed is too slow (Liu et al., 2021). The CFLVAD physiological control systems were designed to adapt to time-varying physiological environment by adjusting pump speed in real time. Therefore, for CFLVAD physiological control, pump regurgitation may also occur when the pump speed is too low. Several CFLVAD multi-objective control systems have been proposed, but whether pump regurgitation should be considered remains controversial. Petrou et al. (2017) constructed a multi-objective physiological control system consisting of five objectives, excluding the objective of pump regurgitation prevention. Wu et al. (2007) argued that preventing pump regurgitation was not necessary for CFLVAD multi-objective physiological control. Leao, Utiyama, Fonseca, Bock, and Andrade (2020) designed a CFLVAD multi-objective physiological control system that considered pump regurgitation and conducted an experiment to prevent pump regurgitation. Pump regurgitation not only causes wasted energy in the CFLVAD battery, but can also lead to recurrent heart failure in patients. We preferred to evaluate the performance of CFLVAD physiological control system through a pump regurgitation prevention experiment. In this study, we tested the performance for the developed physiological control system under extreme condition and did not observe the occurrence of pump regurgitation (Fig. 7).

The design of simulation scenario is an important factor to improve the performance of CFLVAD physiological control system. The CFLVAD physiological control systems constructed in most studies lack neuromodulation function and usually rely on manual setting of parameters to simulate the patient's physiological or active scenario. Fetanat et al. (2021) performed simulations of preload and afterload changes by manually changing the values of vascular resistance, blood volume, and heart rate. Stephens et al. (2021) implemented a simulation of an exercise scenario by directly varying the values of vascular resistance, blood volume, heart rate, and ventricular contractility. Manually setting may cause step change in parameters. In fact, when patients transition from one scenario to another, there is a transition process in the physiological parameters associated with the simulated scenario. In this study, we altered the parameters in the baroreflex system to indirectly regulate the parameters associated with the rest-exercise-rest and rest-sleep-rest scenarios and to realize the transition between the scenarios (Figs. 8 and 9. At rest, exercise, and sleep, CIAPC provided cardiac outputs of approximately 5 L/min, 8 L/min, and 4 L/min, respectively, for a patient with a normal body size. These results are similar to those of the Starling-like control studied by Stephens et al. (2021). Furthermore, this study indicates that the cardiac index followed change in the activity states Figs. 8 and 9. However, this result has not been reported in previous studies on CFLVAD physiologic control.

The cardiovascular system model used in this study had limitation. The cardiovascular system model is the lumped parameter model, which

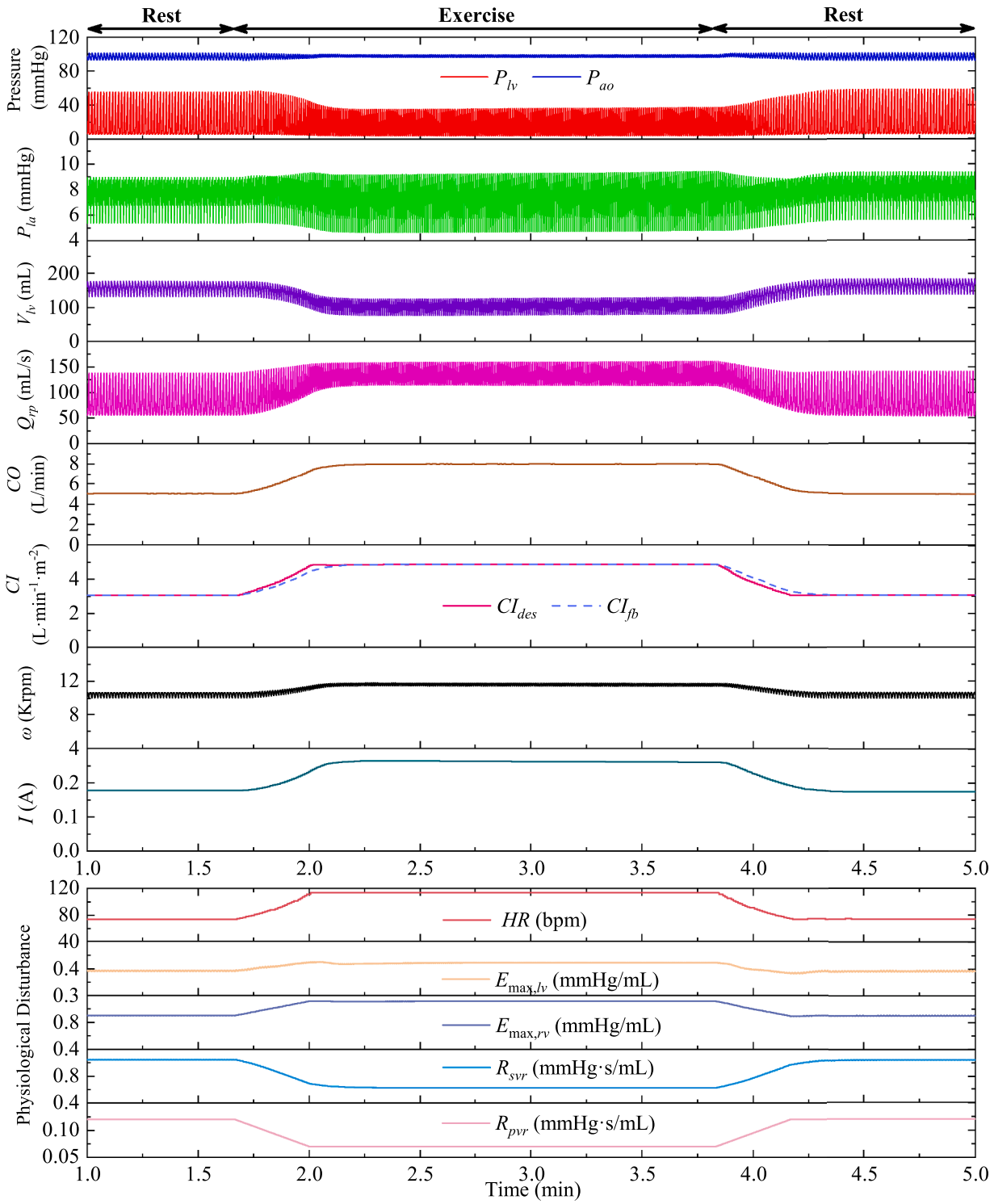

Fig. 8. System responses for CIAPC when the patient is in a rest-exercise-rest scenario. P_{lv} is the left ventricular pressure, P_{la} is the left atrial pressure, P_{ao} is the aortic pressure, V_{lv} is the left ventricular volume, Q_{rp} is the rotary pump flow , ω is the pump speed, I is the current, CO represents the cardiac output, CI_{des} is the desired cardiac index, CI_{fb} is the feedback cardiac index, HR represents the heart rate, $E_{\max,lv}$ is left ventricular end-systolic elastance, $E_{\max,rv}$ is right ventricular end-systolic elastance, R_{pvr} is the left ventricular preload resistance, and R_{svr} is the left ventricular afterload resistance.

assumes that the heart valves are ideal. This means that the modeled valve had no regurgitation, no pressure drop, no gravitational effects, and instantaneous closure. Therefore, the CFLVAD physiological control system in this study could not take the motion state of the aortic valve as a control objective. However, this previously validated cardiovascular system model demonstrates the feasibility of CIAPC for physiologic perfusion, ventricular suction prevention, pump regurgitation prevention, and sensorless control. The effect of CIAPC on the aortic valve can be better verified using the mock circulatory loop and animal model. The present study acknowledges a limitation in its consideration of the interference caused by noise on the signal, particularly regarding the influence of noise from current and pump speed signals. Nonetheless, the impact of this factor on the study's results is deemed relatively minimal, as current and pump speed sensors typically exhibit

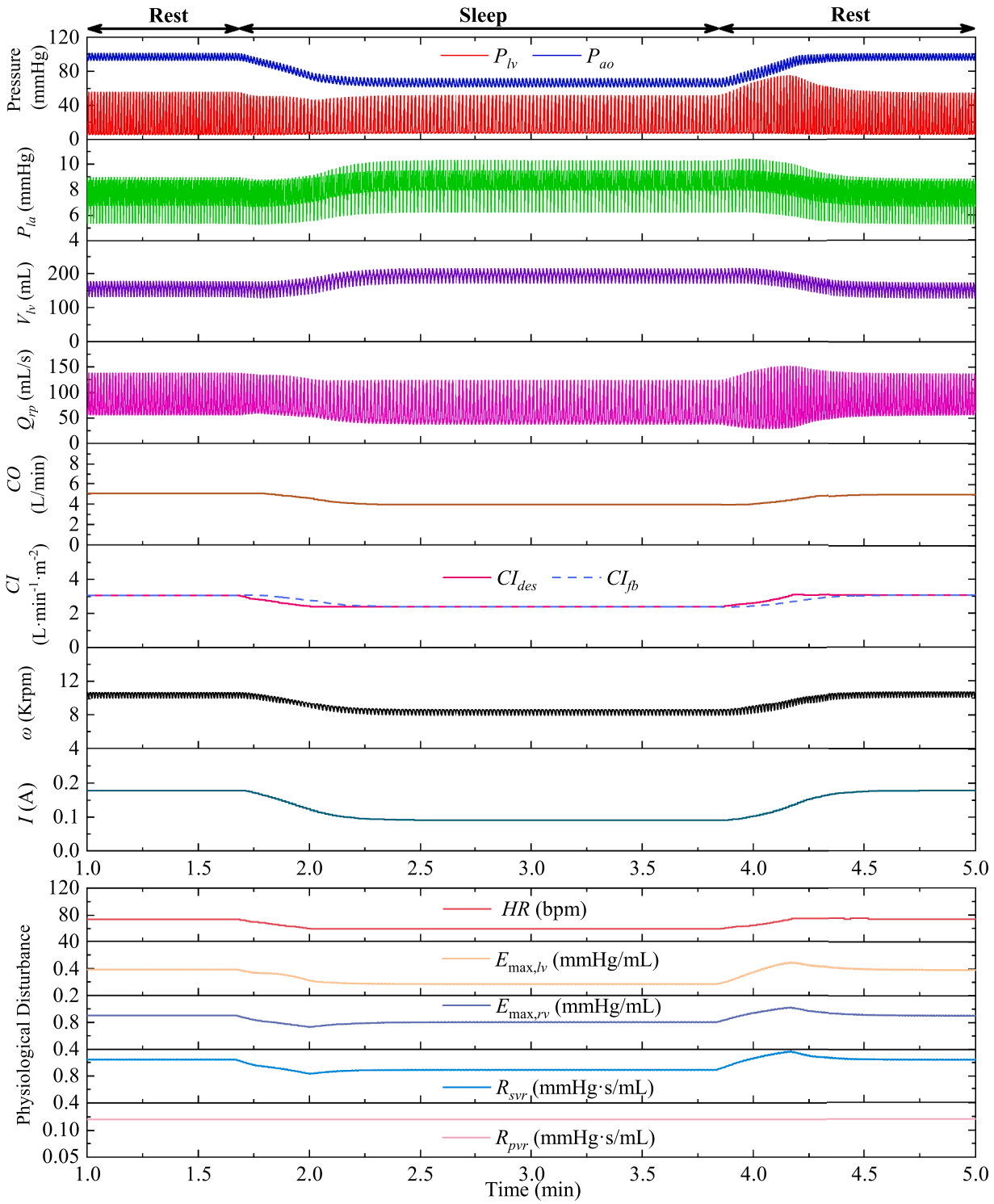

Fig. 9. System responses for CIAPC when the patient is in a rest-sleep-rest scenario. P_{lv} is the left ventricular pressure, P_{la} is the left atrial pressure, P_{ao} is the aortic pressure, V_{lv} is the left ventricular volume, Q_{rp} is the rotary pump flow , ω is the pump speed, I is the current, CO represents the cardiac output, CI_{des} is the desired cardiac index, CI_{fb} is the feedback cardiac index, HR represents the heart rate, $E_{\max,lv}$ is left ventricular end-systolic elastance, $E_{\max,rv}$ is right ventricular end-systolic elastance, R_{pvr} is the left ventricular preload resistance, and R_{svr} is the left ventricular afterload resistance.

a normal distribution of noise that is less than 1 % (Meki et al., 2020). Furthermore, the adverse effects of noise interference can be effectively mitigated through the application of filtering techniques. Another limitation is the use of heart rate as a feedback quantity. In some cases, patients may experience cardiac arrhythmias, which can lead to an imbalance in the rotary pump flow supply. This study, in particular, did not establish a synchronization between the ventricular elasticity model and the QRS complex in the electrocardiogram (ECG). This lack of synchronization may diminish the effectiveness of this strategy in cases of arrhythmia. The next phase will involve the development of a QRS complex detection function, which will subsequently be followed by the application of synthetic ECGs to assess the efficacy of the CIAPC strategy.

Furthermore, If a stable heart rate is missing for a long period of time, CFLVAD should be switched to a constant speed to avoid problems caused by cardiac arrhythmia.

5. Conclusion

The CIAPC strategy proposed in this study realized the personalized CFLVAD therapy. In addition, CIAPC not only provided suitable physiological perfusion for patients with different body types, but also prevented ventricular suction and pump regurgitation under extreme conditions. CIAPC ensured smooth switching between different scenarios and could adjust the patient's cardiac index and cardiac output in real time according to the patient's activity state. In the next study, we will further verify the practicality of CIAPC through in vitro experiments.

CRediT authorship contribution statement

Hongtao Liu: Conceptualization, Writing – original draft, Investigation, Methodology, Project administration, Supervision; **Aili Guan:** Conceptualization, Writing – original draft, Investigation, Methodology, Resources, Formal analysis; **Fayu Xing:** Conceptualization, Writing – original draft, Investigation, Methodology, Resources, Formal analysis; **Yunpeng Zhang:** Writing – original draft, Methodology, Validation; **Wencheng Wang:** Writing – review & editing, Software, Project administration, Data curation; **Guoxu Liu:** Writing – review & editing, Software, Data curation.

Declaration of competing interest

The authors declare that they have no known competing financial interests or personal relationships that could have appeared to influence the work reported in this paper.

Data availability

Data will be made available on request.

Acknowledgment

This work was supported in part by the Natural Science Foundation of Shandong (CN) under Grant ZR2023QF139 and Grant ZR2023MF047; and in part by the Doctoral Starting Up Foundation of Weifang University under Grant 2023BS44.

References

Bakouri, M., & Sikkandar, M. Y. (2020). Numerical investigation on preload and afterload sensitivity for using ventricular assist device on heart failure patients. *Journal of Mechanics in Medicine and Biology*, *20*(7), 1–15. https://doi.org/10.1142/S0219519420500426

Belkin, M. N., Kagan, V., Labuhn, C., Pinney, S. P., & Grinstein, J. (2022). Physiology and clinical utility of heartmate pump parameters. *Journal of Cardiac Failure*, *28*(5), 845–862. https://doi.org/10.1016/j.cardfail.2021.11.016

Bozkurt, S., van Tuijl, S., Schampaert, S., van de Vosse, F. N., & Rutten, M. C. M. (2014). Arterial pulsatility improvement in a feedback-controlled continuous flow left ventricular assist device: An ex-vivo experimental study. *Medical Engineering & Physics*, *36*(10), 1288–1295. https://doi.org/10.1016/j.medengphy.2014.07.005

Bozkurt, S., van Tuijl, S., van de Vosse, F. N., & Rutten, M. C. M. (2016). Arterial pulsatility under phasic left ventricular assist device support. *Bio-Medical Materials and Engineering*, *27*(5), 451–460. https://doi.org/10.3233/bme-161599

Choi, S., Boston, J. R., Thomas, D., & Anta, J. F. (1997). Modeling and identification of an axial flow blood pump. In *Proceedings of the American Control Conference* (pp. 3714–3715).

Dual, S. A., Anthamatten, L., Shah, P., Meboldt, M., & Schmid Daners, M. (2020). Ultrasound-based prediction of interventricular septum positioning during left ventricular support-an experimental study. *Journal of Cardiovascular Translational Research*, *13*(6), 1055–1064. https://doi.org/10.1007/s12265-020-10034-3

Fetanat, M., Stevens, M., Hayward, C., & Lovell, N. H. (2020). A physiological control system for an implantable heart pump that accommodates for interpatient and intrapatient variations. *IEEE Transactions on Biomedical Engineering*, *67*(4), 1167–1175. https://doi.org/10.1109/tbme.2019.2932233

Fetanat, M., Stevens, M., Hayward, C., & Lovell, N. H. (2021). A sensorless control system for an implantable heart pump using a real-time deep convolutional neural network. *IEEE Transactions on Biomedical Engineering*, *68*(10), 3029–3038. https://doi.org/10.1109/TBME.2021.3061405

Gao, B., Chang, Y., Gu, K., Zeng, Y., & Liu, Y. (2012). A pulsatile control algorithm of continuous-flow pump for heart recovery. *ASAIO Journal*, *58*(4), 343–352. https://doi.org/10.1097/MAT.0b013e318256bb76

Habigt, M. A., Gesenhues, J., Ketelhut, M., Hein, M., Duschner, P., Rossaint, R., & Mechelinck, M. (2021). In vivo evaluation of two adaptive starling-like control algorithms for left ventricular assist devices. *Biomedical Engineering-Biomedizinische Technik*, *66*(3), 257–266. https://doi.org/10.1515/bmt-2020-0248

Hildebrand, S., Diedrich, M., Brockhaus, M., Finocchiaro, T., Cuenca, E., De Ben, H., Steinseifer, U., Schmitz-Rode, T., & Jansen, S. V. (2022). Controlling the flow balance: In vitro characterization of a pulsatile total artificial heart in preload and afterload sensitivity. *Artificial Organs*, *46*(1), 71–82. https://doi.org/10.1111/aor.14042

Jing, T., Xin, T. Y., Wang, F. Q., Zhang, Z. H., & Zhou, L. (2022). Control strategy design of a microblood pump based on heart-rate feedback. *Micromachines*, *13*(3), 1–15. https://doi.org/10.3390/mi13030358

Kilic, A., Kwon, J. H., Grady, K. L., Singletary, B. A., Kilic, A., Everitt, M., Cleveland, J., Cantor, R. S., Blackmon, S., Breathett, K., McKellar, S., Keebler, M., Kirklin, J. K., & Stehlik, J. (2023). Impact of adverse events on health-related quality of life after left ventricular assist device implantation: An STS INTERMACS analysis. *Journal of Heart and Lung Transplantation*, *42*(9), 1214–1222. https://doi.org/10.1016/j.healun.2023.04.001

Leao, T., Utiyama, B., Fonseca, J., Bock, E., & Andrade, A. (2020). In vitro evaluation of multi-objective physiological control of the centrifugal blood pump. *Artificial Organs*, *44*(8), 785–796. https://doi.org/10.1111/aor.13639

Liang, L., Meki, M., Wang, W., Sethu, P., El-Baz, A., Giridharan, G. A., & Wang, Y. (2020). A suction index based control system for rotary blood pumps. *Biomedical Signal Processing And Control*, *62*, 1–8. 1746–8094

Liu, H., Liu, S., Ma, X., & Zhang, Y. (2020). A numerical model applied to the simulation of cardiovascular hemodynamics and operating condition of continuous-flow left ventricular assist device. *Mathematical Biosciences and Engineering*, *17*(6), 7519–7543. https://doi.org/10.3934/mbe.2020384

Liu, H. T., Liu, S. Q., & Ma, X. X. (2021). Varying speed modulation of continuous-flow left ventricular assist device based on cardiovascular coupling numerical model. *Computer Methods in Biomechanics and Biomedical Engineering*, *24*(9), 956–972. https://doi.org/10.1080/10255842.2020.1861601

Mancini, D., & Colombo, P. C. (2015). Left ventricular assist devices a rapidly evolving alternative to transplant. *Journal of the American College of Cardiology*, *65*(23), 2542–2555. https://doi.org/10.1016/j.jacc.2015.04.039

Maw, M., Schlöglhofer, T., Marko, C., Aigner, P., Gross, C., Widhalm, G., Schaefer, A. K., Schima, M., Wittmann, F., Wiedemann, D., Moscato, F., Kudlik, D., Stadler, R., Zimpfer, D., & Schima, H. (2022). A sensorless modular multiobjective control algorithm for left ventricular assist devices: A clinical pilot study. *Frontiers in Cardiovascular Medicine*, *9*, 11. https://doi.org/10.3389/fcvm.2022.888269

Meki, M., Wang, Y., Sethu, P., Ghazal, M., El-Baz, A., & Giridharan, G. (2020). A sensorless rotational speed-based control system for continuous flow left ventricular assist devices. *IEEE Transactions on Biomedical Engineering*, *67*(4), 1050–1060. https://doi.org/10.1109/Tbme.2019.2928826

Molina, E. J., Shah, P., Kiernan, M. S., Cornwell, W. K., Copeland, H., Takeda, K., Fernandez, F. G., Badhwar, V., Habib, R. H., Jacobs, J. P., Koehl, D., Kirklin, J. K., Pagani, F. D., & Cowger, J. A. (2021). The society of thoracic surgeons intermacs 2020 annual report. *Annals of Thoracic Surgery*, *111*(3), 778–792. https://doi.org/10.1016/j.athoracsur.2020.12.038

Ng, B. C., Salamonsen, R. F., Gregory, S. D., Stevens, M. C., Wu, Y., Mansouri, M., Lovell, N. H., & Lim, E. (2018). Application of multiobjective neural predictive control to biventricular assistance using dual rotary blood pumps. *Biomedical Signal Processing and Control*, *39*, 81–93. https://doi.org/10.1016/j.bspc.2017.07.028

Ng, B. C., Smith, P. A., Nestler, F., Timms, D., Cohn, W. E., & Lim, E. (2017). Application of adaptive starling-like controller to total artificial heart using dual rotary blood pumps. *Annals of Biomedical Engineering*, *45*(3), 567–579. https://doi.org/10.1007/s10439-016-1706-3

Ochsner, G., Amacher, R., Wilhelm, M. J., Vandenberghe, S., Tevaearai, H., Plass, A., Amstutz, A., Falk, V., & Daners, M. S. (2014). A physiological controller for turbodynamic ventricular assist devices based on a measurement of the left ventricular volume. *Artificial Organs*, *38*(7), 527–538. https://doi.org/10.1111/aor.12225

Pauls, J. P., Stevens, M. C., Bartnikowski, N., Fraser, J. F., Gregory, S. D., & Tansley, G. (2016a). Evaluation of physiological control systems for rotary left ventricular assist devices: An in-vitro study. *Annals of Biomedical Engineering*, *44*(8), 2377–2387. https://doi.org/10.1007/s10439-016-1552-3

Pauls, J. P., Stevens, M. C., Schummy, E., Tansley, G., Fraser, J. F., Timms, D., & Gregory, S. D. (2016b). In vitro comparison of active and passive physiological control systems for biventricular assist devices. *Annals of Biomedical Engineering*, *44*(5), 1370–1380. https://doi.org/10.1007/s10439-015-1425-1

Petrou, A., Monn, M., Meboldt, M., & Daners, M. S. (2017). A novel multi-objective physiological control system for rotary left ventricular assist devices. *Annals of Biomedical Engineering*, *45*(12), 2899–2910. https://doi.org/10.1007/s10439-017-1919-0

Pillay, P., & Krishnan, R. (1989). Modeling, simulation, and analysis of permanent-magnet motor-drives .2. The brushless DC motor drive. *IEEE Transactions on Industry Applications*, *25*(2), 274–279. https://doi.org/10.1109/28.25542

Stephens, A., Gregory, S., Tansley, G., Busch, A., & Salamonsen, R. (2019a). In vitro evaluation of an adaptive starling-like controller for dual rotary ventricular assist devices. *Artificial Organs*, *43*(11), E294–E307. https://doi.org/10.1111/aor.13510

Stephens, A. F., Busch, A., Salamonsen, R. F., Gregory, S. D., & Tansley, G. D. (2021). Rotary ventricular assist device control with a fiber BRAGG grating pressure sensor.

IEEE Transactions on Control Systems Technology, *29*(3), 1009–1018. https://doi.org/10.1109/tcst.2020.2989692

Stephens, A. F., Gregory, S. D., Burrell, A. J. C., Marasco, S., Stub, D., & Salamonsen, R. F. (2020). Physiological principles of starling-like control of rotary ventricular assist devices. *Expert Review of Medical Devices*, *17*(11), 1169–1182. https://doi.org/10.1080/17434440.2020.1841631

Stephens, A. F., Gregory, S. D., & Salamonsen, R. F. (2019b). The importance of venous return in starling-like control of rotary ventricular assist devices. *Artificial Organs*, *43*(3), E16–E27. https://doi.org/10.1111/aor.13342

Stephens, A. F., Stevens, M. C., Gregory, S. D., Kleinheyer, M., & Salamonsen, R. F. (2017). In vitro evaluation of an immediate response starling-like controller for dual rotary blood pumps. *Artificial Organs*, *41*(10), 911–922. https://doi.org/10.1111/aor.12962

Tanner, G.A., & Rhoades, R. (2003). Medical physiology. (2nd Edition). Indianapolis: Lippincott Williams & Wilkins.

Tchantchaleishvili, V., Luc, J. G. Y., Cohan, C. M., Phan, K., Hübbert, L., Day, S. W., & Masey, H. T. (2017). Clinical implications of physiologic flow adjustment in continuous-flow left ventricular assist devices. *ASAIO Journal*, *63*(3), 241–250. https://doi.org/10.1097/mat.0000000000000477

Wang, F. Q., Wang, S. J., Li, Z. J., He, C. Y., Xu, F., & Jing, T. (2022). A non-invasive physiological control system of a rotary blood pump based on preload sensitivity: Use of frank-starling-like mechanism. *Micromachines*, *13*(11), 1–11. https://doi.org/10.3390/mi13111981

Wang, Y., Koenig, S. C., Slaughter, M. S., & Giridharan, G. A. (2015). Rotary blood pump control strategy for preventing left ventricular suction. *ASAIO Journal*, *61*(1), 21–30. https://doi.org/10.1097/mat.0000000000000152

Weissler, A. M., Harris, W. S., & Schoenfeld, C. D. p. C. (1968). Systolic time intervals in heart failure in man. *Circulation*, *37*(2), 149–159. https://doi.org/10.1161/01.CIR.37.2.149

Wu, E. L., Stevens, M. C., Nestler, F., Pauls, J. P., Bradley, A. P., Tansley, G., Fraser, J. F., & Gregory, S. D. (2020). A starling-like total work controller for rotary blood pumps: An in vitro evaluation. *Artificial Organs*, *44*(3), E40–E53. https://doi.org/10.1111/aor.13570

Wu, Y., Allaire, P. E., Tao, G., & Olsen, D. (2007). Modeling, estimation, and control of human circulatory system with a left ventricular assist device. *IEEE Transactions on Control Systems Technology*, *15*(4), 754–767. https://doi.org/10.1109/tcst.2006.890288

Wu, Y., & Zheng, Q. (2015). AdRC or adaptive controller - a simulation study on artificial blood pump. *Computers in Biology and Medicine*, *66*, 135–143. https://doi.org/10.1016/j.compbiomed.2015.09.006

Yu, C.-Y., Lin, C.-H., & Yang, Y.-H. (2010). Human body surface area database and estimation formula. *Burns : Journal of the International Society for Burn Injuries*, *36*(5), 616–629. https://doi.org/10.1016/j.burns.2009.05.013